AMPP™
ANNUAL CONFERENCE + EXPO
MARCH 3-7, 2024 | NEW ORLEANS, LOUISIANA

Effect of Sample Configuration on Autoclave Experiment in Dense Phase CO_2 with Impurities

Xi Wang
Ohio University
342 W State Street
Athens, Ohio, 45701
USA

Yoon-Seok Choi
Ohio University
342 W State Street
Athens, Ohio, 45701
USA

Gaoxiang (Garret) Wu
ExxonMobil Technology and Engineering
Company
22777 Springwoods Village Parkway
Spring, Texas, 77389
USA

Srdjan Nesic
Ohio University
342 W State Street
Athens, Ohio, 45701
USA

ABSTRACT

Corrosion plays an important role in the integrity management of the CO_2 transport pipeline, since carbon steels, the most common material utilized for pipeline construction, are susceptible to corrosion in the presence of impurities, such as water, SO_2, and NO_2. Autoclave tests have been used to examine the corrosion susceptibility and severity in this condition. However, studies have shown a range of corrosion rates in similar experimental conditions, and there are no standard methods for laboratory corrosion testing in dense phase CO_2 with impurities. In this study, the impact of sample configuration, one of the parameters that can affect the results of the corrosion experiment, is investigated. Autoclave experiments were conducted in dense phase CO_2 with O_2, SO_2, NO_2, H_2S, CH_4, and H_2O where the samples were placed either vertically or horizontally. Furthermore, horizontal samples were placed in different locations of the autoclave. The results showed that corrosion was observed on both sides of the vertical samples, while top side of each horizontal sample corroded more compared to the bottom side in some conditions. For horizontal samples, the corrosion rates could increase with the location from top to bottom of the autoclave depending on the combination of impurities.

Key words: CO_2 transport, carbon capture and storage, dense phase CO_2

INTRODUCTION

Corrosion plays an important role in the integrity management of the CO_2 transport pipeline since carbon steels, the most common material utilized for pipeline construction, are susceptible to corrosion in the presence of water.

It is well known that dry CO_2 does not corrode carbon steels, and negligible corrosion occurs at water-unsaturated conditions (below the solubility level) in dense phase CO_2 (liquid and supercritical). However, recent studies have reported that noticeable, and potentially severe, corrosion occurs at water-unsaturated conditions in dense phase CO_2 with the presence of impurities, such as O_2, H_2S, SO_2, NO_2, etc. due to interactions between chemical species that are not properly understood. Therefore, experimental works have been carried out to understand the corrosion risks associated with the dense phase CO_2 system[1–5]. Carbon steel samples have been used in autoclave setups, but the corrosion rates from different apparatuses could vary even for similar conditions. Morland and Svenningsen pointed out the importance of proper CO_2 injection during experiment[6]. In addition to the injection procedure, the sample configurations, such as sample location in the autoclave, are often omitted in the experimental design, which could cause result variation as well.

The objective of this work is to investigate the impact of sample configuration on its corrosion rate in the dense phase CO_2 environment via exposure experiments and post-exposure surface characterizations with scanning electron microscopy (SEM), energy dispersive X-ray spectroscopy (EDS), and Raman spectroscopy.

EXPERIMENTAL PROCEDURE

API 5L X65 carbon steel was machined into a rectangular type with a size of 3.8 cm × 1.3 cm × 0.3 cm. Prior to exposure, the specimens were grounded sequentially with #180, #400, and #600 grit silicon carbide paper with water flow. They were rinsed with deionized (DI) water, sonicated in an isopropyl alcohol bath for 60 seconds, and dried with lab air.

Corrosion tests were carried out in a high-pressure system, consisting of a 5 L Hastelloy autoclave, impurity injection/analysis system, and CO_2 booster pump. Specimens were placed in the autoclave and the heated autoclave was purged with dry CO_2 for 1 hour to remove any oxygen and humidity. After the autoclave cooled down with continuous dry CO_2 ingress, the dry CO2 ingress was stopped, and the desired amount of deoxygenated DI water was added to the autoclave prior to adding other impurities. Once the autoclave was sealed, the autoclave temperature was adjusted to the test temperature, 25 °C. Then, the impurity gases were introduced to the autoclave using the gas injection system. The impurities were added from technical grade (ultra-high purity) SO_2, NO_2, H_2S, CH_4, N_2, and O_2 cylinders with a custom-built gas injection system. For NO_2 and CH_4, a mixture with CO_2 was used. For trace quantity of each impurity gas, the required number of moles of gas required in the autoclave was obtained by first injecting the gas into a cylinder of known volume at a known temperature and pressure. The gas was then "pushed" into the autoclave with CO_2. The moles of each impurity required to reach the required concentrations were calculated from the Peng-Robinson equation of state. The impurities were injected into the autoclave separately one by one. The sequence of impurity injection was following the order: H_2O, CH_4, N_2, H_2S, SO_2, O_2, NO_2. High pressure CO_2 sourced from high-purity bottles was added to the autoclave aided with a gas booster pump to achieve the desired working pressure.

In order to track the impurity concentration during the test, the concentration of impurities was measured with a gas detector tube by taking a small volume sample of the mixture from the autoclave daily. The measurement error is +/- 10%. Impurities were not replenished during the test.

Table 1 shows the test matrix for the present study. Four corrosion tests were performed with 2 different sample configurations as shown in Figure 1. Tests 1 and 2 were conducted with in total two vertical positioned X65 specimens (Figure 1a) whereas Tests 3 and 4 were performed with in total six horizontal positioned X65 specimens at different locations in the autoclave (Figure 1b).

The water solubility limit at the testing pressure and temperature is above 3000 ppm in the dense phase CO_2[7]. In order to make sure all impurities distributed homogeneously inside the experimental chamber instead of phasing out in the undissolved water, water contents were controlled to be lower than 3000 ppm in this work (200 ppm and 1000 ppm). The ppm unit used in the present study represents mole basis concentration.

Table 1
Test matrix for the corrosion test

Test No.	T (^{o}C)	P(bar)	CO_2	O_2 (ppm)	H_2S (ppm)	SO_2 (ppm)	NO_2 (ppm)	CH_4 (ppm)	H_2O (ppm)	N_2 (ppm)	Period (day)
1	25	100	Bal	100	100	100	100	100	200	500	2
2	25	100	Bal	100	100	100	100	100	1000	500	2
3	25	100	Bal	100	100	100	100	100	200	500	2
4	25	100	Bal	100	100	100	0	100	1000	500	2
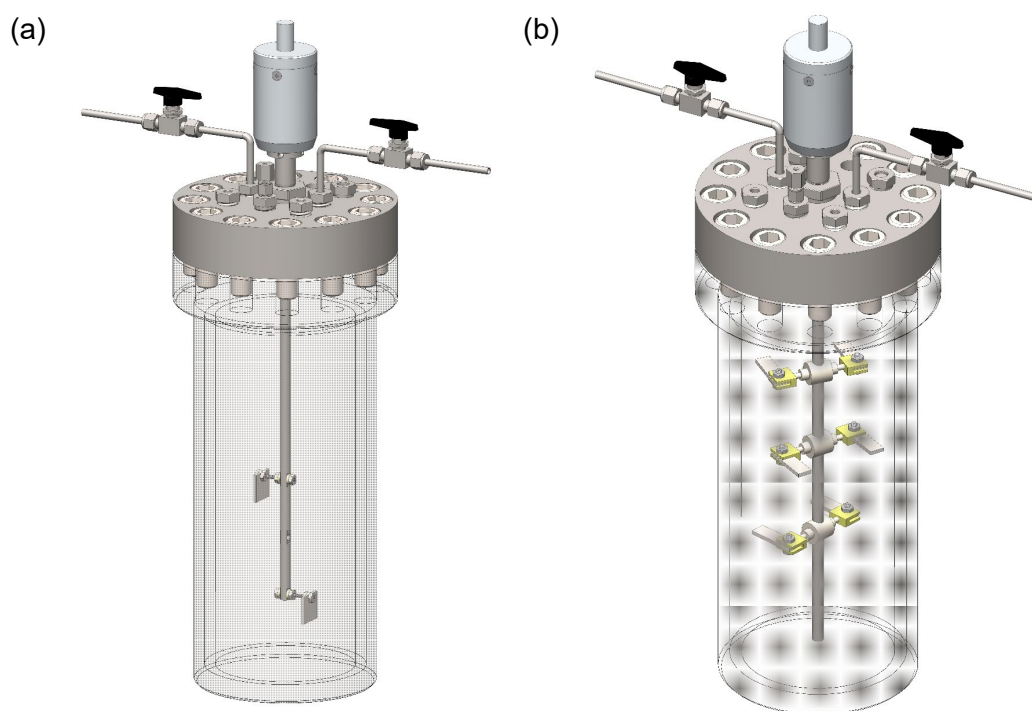
Figure 1: Schematic of sample layouts in the 5L autoclave: (a) two-sample vertical arrangement, (b) six-sample horizontal arrangement. Samples were arranged to not overlap with each other.

Uniform corrosion rate of carbon steel was measured by weight loss (WL) method at the end of 48 hours exposure. After surface analysis, the samples were cleaned by using Clarke's solution per ASTM[1] G1[8]. The samples were then rinsed in DI water and isopropanol, dried, and weighed to 0.1 mg. The average corrosion rate during the test period was calculated by the following equation:

---

[1] ASTM International, 100 Barr Harbor Dr., West Conshohocken, PA 19428-2959.

$$\text{Corrosion rate (mm/year)} = \frac{8.76 \times 10^4 \times \text{weight loss (g)}}{\text{area (cm}^2) \times \text{density (g/cm}^3) \times \text{time (hour)}}$$

After each test, corrosion product layers were analyzed using a variety of surface analytical tools, including SEM, EDS, and Raman microscopy, to characterize corrosion product morphology and composition.

RESULTS AND DISCUSSION

Vertical Samples

Two vertical X65 specimens were exposed to dense phase CO_2 (100 bar and 25°C) in Test 1 (with 200 ppm water and 100 ppm of O_2, H_2S, SO_2, NO_2, and CH_4) and Test 2 (with 1000 ppm water and 100 ppm of O_2, H_2S, SO_2, NO_2, and CH_4). The samples were placed vertically in these tests. The photos of specimens after exposure and after cleaning are illustrated in Figure 2. The post exposure samples (Figure 2, before cleaning) were covered with dark corrosion products. Localized corrosion was not observed on any of the samples after removing the corrosion products. The corrosion rate of the Test 1 upper sample was 0.08 mm/year, and the lower one was 0.28 mm/year. The corrosion rate of the Test 2 upper sample was 0.06 mm/year, and the lower sample corrosion rate was 0.07 mm/year.
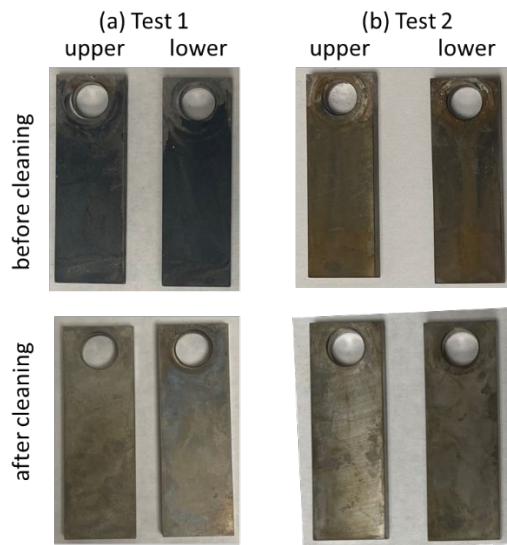
Figure 2: Photos of (a) Test 1 and (b) Test 2 vertical samples before and after cleaning. "Upper" and "lower" are the locations where the samples were in the autoclave.

The surface morphology and corrosion products were examined with SEM and EDS. One characteristic area of each test is shown in Figure 3. Test 1 sample in Figure 3a featured nodule-like bright spots, a thick corrosion product layer, and a thin corrosion product layer. These were analyzed by using EDS, and they were all enriched with C, S, O, and Fe. Test 2 sample in Figure 3b had less corrosion product accumulation than Test 1 sample, since the polishing lines were still visible (Figure 3b, 500x magnification), not covered by corrosion products. Elemental analysis showed that both the nodule-like spots and the surface corrosion product layer were composed of Fe, S, O, and C, likely $FeSO_4$ and $FeCO_3$.

(a) Test 1

Element	At. No.	Mass [%]	Mass Norm. [%]	Atom [%]	abs. error [%] (3 sigma)
C	6	1.22	1.44	5.15	1.17
O	8	7.40	8.69	23.40	3.55
S	16	3.12	3.66	4.92	0.51
Fe	26	73.39	86.21	66.52	6.93
		85.13	100.00	100.00	

Element	At. No.	Mass [%]	Mass Norm. [%]	Atom [%]	abs. error [%] (3 sigma)
C	6	0.53	0.66	2.52	0.68
O	8	4.99	6.17	17.74	2.49
S	16	3.97	4.90	7.03	0.59
Fe	26	71.45	88.27	72.71	6.67
		80.95	100.00	100.00	

Element	At. No.	Mass [%]	Mass Norm. [%]	Atom [%]	abs. error [%] (3 sigma)
C	6	0.57	0.67	2.79	0.83
O	8	2.27	2.65	8.35	1.57
S	16	2.01	2.34	3.68	0.43
Mn	25	0.87	1.01	0.93	0.50
Fe	26	80.03	93.33	84.25	7.65
		85.75	100.00	100.00	

(b) Test 2

Element	At. No.	Mass [%]	Mass Norm. [%]	Atom [%]	abs. error [%] (3 sigma)
C	6	1.02	1.38	4.31	0.99
O	8	9.60	13.08	30.57	4.20
S	16	11.58	15.77	18.40	1.37
Fe	26	51.24	69.77	46.73	4.87
		73.44	100.00	100.00	

Element	At. No.	Mass [%]	Mass Norm. [%]	Atom [%]	abs. error [%] (3 sigma)
C	6	1.04	1.26	5.04	1.06
O	8	2.98	3.60	10.83	1.79
S	16	2.81	3.40	5.10	0.50
Fe	26	75.83	91.74	79.03	7.16
		82.65	100.00	100.00	

Element	At. No.	Mass [%]	Mass Norm. [%]	Atom [%]	abs. error [%] (3 sigma)
C	6	1.17	1.39	5.62	1.14
O	8	2.73	3.23	9.79	1.69
S	16	2.17	2.57	3.89	0.43
Fe	26	78.38	92.81	80.69	7.39
		84.46	100.00	100.00	

Figure 3: SEM/EDS analysis of (a) Test 1 and (b) Test 2 corrosion products

To further identify the corrosion product, Raman spectroscopy was performed. Pronounced peaks of matching $FeSO_4$ and S references were found as shown in Figure 4. $FeSO_4$ is a corrosion product from sulfuric acid corrosion, which is generated from the reactions between impurities in the dense phase CO_2.
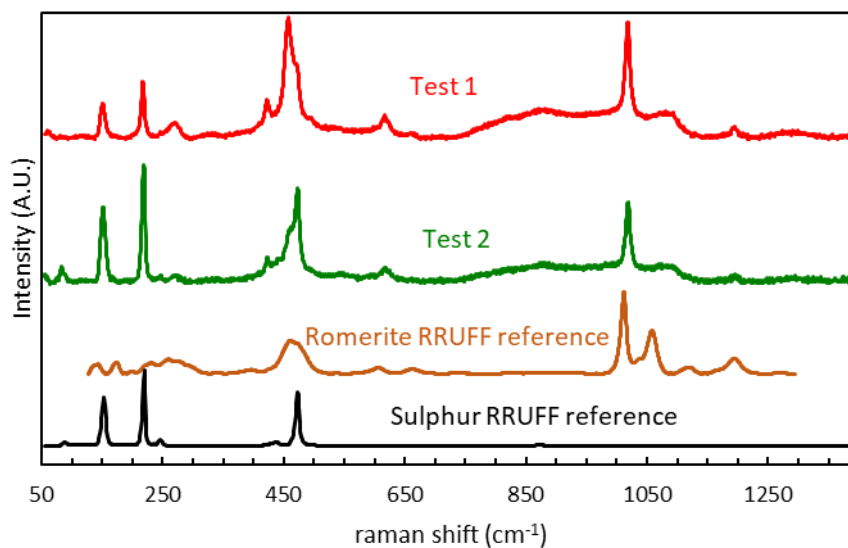
Figure 4: Raman spectroscopy of surface corrosion products after Test 1 and 2. FeSO4 reference spectrum is indexed as "Romerite R060820", and elemental sulphur reference spectrum is indexed as "Sulphur R040135-3" in the RRUFF database[9].

The impurities in the dense phase CO_2 reacted with each other and could form H_2SO_4 and S following the below reactions[2, 10]:

$$SO_2 + \frac{1}{2}O_2 + H_2O \rightleftharpoons H_2SO_4 \tag{1}$$

$$SO_2 + H_2O + NO_2 \rightleftharpoons NO + H_2SO_4 \tag{2}$$

$$2NO + O_2 \rightleftharpoons 2NO_2 \tag{3}$$

$$H_2S + 3NO_2 \rightleftharpoons SO_2 + H_2O + 3NO \tag{4}$$

$$H_2S + H_2SO_4 \rightleftharpoons S + SO_2 + 2H_2O \tag{5}$$

$$3H_2S + 2HNO_3 \rightleftharpoons 3S + 2NO + 4H_2O \tag{6}$$
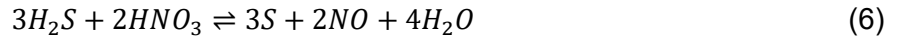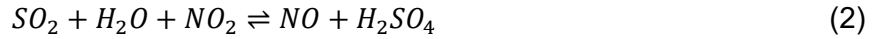
The corresponding change of the measured impurities will be discussed later in the paper.

To investigate whether the corrosion rate difference between the upper and lower samples was an experimental error or an actual effect due to sample position inside the autoclave, the samples were placed horizontally at three levels in the autoclave in the next two tests as illustrated in Figure 1b.

Horizontal Samples
Test 3 is a repeat of Test 1, where samples were exposed to liquid CO_2 at 25 °C with 200 ppm water and 100 ppm of O_2, H_2S, SO_2, NO_2, and CH_4. Figure 5a demonstrates post-exposure photos of samples with both faces of each sample. The facing up sides of all 3 levels (Figure 5a, facing up, top/middle/bottom) were covered with greenish corrosion products. Visually, the bottom sample did have more corrosion products than the top and middle samples. The facing down sides (Figure 5a, facing down, top/middle/bottom) were shiny with some discolorations. After removing the corrosion products, the facing up sides (Figure 5b) were dull, while the facing down sides were shiny with little corrosion marks. Although the appearances of samples at different levels were different, the corrosion rates of them were close, and the average corrosion rate was about 0.10 mm/year.

During depressurization of the autoclave, although it was slowly depressurized (roughly 400 psi per hour), the autoclave temperature still decreased to around 10 °C. In order to understand whether the thicker corrosion product on the bottom sample formed during the pressurized dense phase CO_2 condition or formed during depressurization where H_2SO_4 could drop out, a similar experiment was conducted but without NO_2, since NO_2 is important to support efficient H_2SO_4 formation according to reaction (2).

Six test specimens were used in Test 4 with 100 ppm O_2, H_2S, SO_2, CH_4 and 1000 ppm water in supercritical CO_2 at 25 °C. This condition was close to Test 2, but without NO_2. The samples were placed horizontally, so both sides of each sample were pictured after rinsing with isopropanol and DI water as shown in Figure 5c. The samples were covered with a thick layer of corrosion products regardless of the position or sides. Some of the observed corrosion products changed from black to orange color shortly after being taken out of the autoclave. After cleaning the surface corrosion products, both sides of all samples were dull, clearly experienced uniform corrosion without any localized attack as shown in Figure 5d. In addition, the average corrosion rate of the bottom samples was around 0.37 mm/year, twice that of the middle and top samples around 0.18 and 0.16 mm/year, respectively.

Figure 5: Photos of Test 3 and Test 4 samples before and after cleaning. "Facing up" and "facing down" indicate the two sides of the same sample. "Top", "Middle", and "Bottom" are the locations of samples inside the autoclave during test.

The surface morphology of all positions and both sides of Test 3 samples before removing the corrosion products are demonstrated in Figure 6. The facing up sides showed more corrosion products than the facing down sides. The corrosion products were composed of C, O, S, Fe, likely $FeCO_3$ and $FeSO_4$. Although the as-cleaned surface of Test 3 facing down sides of specimens were shiny in Figure 5b, Figure 6b showed dimples on the surface in addition to the thin layer of corrosion products. Corrosion happened on both sides of the specimen, but more corrosion products accumulated on the facing up sides. Given the fact that the corrosion rates were close across the positions, the thick corrosion product on the bottom sample could be an artifact due to H_2SO_4 phasing out during depressurization.

(a) Bottom facing up
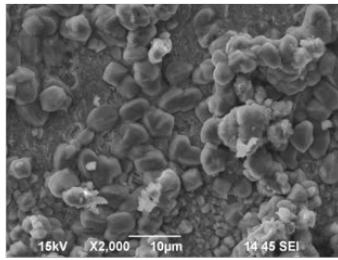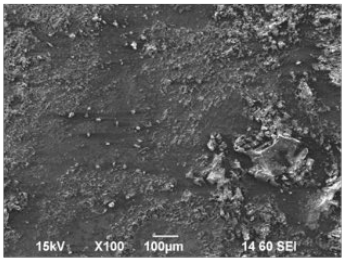
Element	At. No.	Mass [%]	Mass Norm. [%]	Atom [%]	abs. error [%] (3 sigma)
C	6	1.05	1.55	4.08	0.56
O	8	13.52	19.82	39.24	4.59
S	16	19.57	28.68	28.34	2.08
Fe	26	34.08	49.95	28.34	3.02
		68.23	100.00	100.00	

(b) Bottom facing down
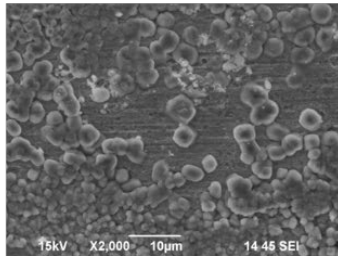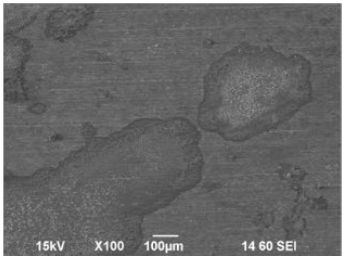
Element	At. No.	Mass [%]	Mass Norm. [%]	Atom [%]	abs. error [%] (3 sigma)
C	6	0.47	0.71	2.10	0.44
O	8	7.92	11.85	26.36	3.10
S	16	22.39	33.51	37.19	2.39
Fe	26	36.03	53.93	34.36	3.27
		66.81	100.00	100.00	

Figure 6: SEM/EDS analysis of Test 3 bottom sample corrosion products.

The appearance of the corrosion products in Test 4 (Figure 7) was clearly different from Test 3 (Figure 6). Test 4 corrosion product was macroscopically in dark color or orange color due to oxidation and was more chalky-look under SEM compared to Test 3. The corrosion product was composed of C, S, O, and Fe, but the C content was considerably lower than other elements. Considering the reactions that could happen between impurities, the corrosion products could be $FeSO_4$ or iron sulfide (FeS).

(a) Bottom facing up
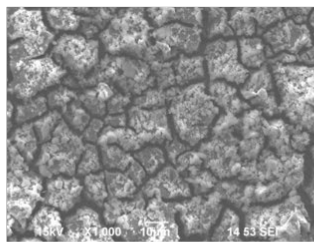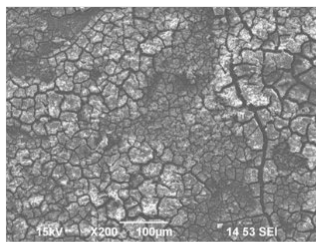
Element	At. No.	Mass [%]	Mass Norm. [%]	Atom [%]	abs. error [%] (3 sigma)
C	6	1.13	1.46	4.77	0.99
O	8	6.23	8.05	19.72	2.83
S	16	17.79	22.99	28.11	2.02
Fe	26	52.24	67.50	47.40	4.87
		77.39	100.00	100.00	

(b) Bottom facing down
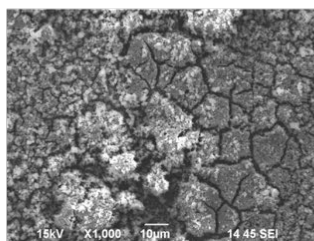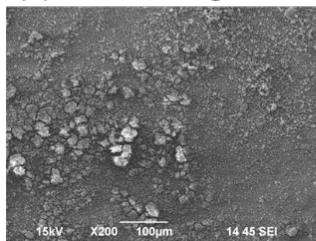
Element	At. No.	Mass [%]	Mass Norm. [%]	Atom [%]	abs. error [%] (3 sigma)
C	6	0.58	0.72	2.47	0.62
O	8	6.75	8.42	21.53	2.89
S	16	13.85	17.27	22.05	1.59
Fe	26	59.03	73.59	53.95	5.41
		80.21	100.00	100.00	

Figure 7: SEM/EDS analysis of Test 4 middle sample corrosion products.

To further identify the corrosion product, Raman spectroscopy was used to examine Test 4 samples. The detected Raman peaks (Figure 8) corresponded with mackinawite. The interaction volume of Raman laser is small, and only provides the information of the outer layer of the corrosion products. The detected O content in Figure 7 could be resulted from either the oxidation of mackinawite or the $FeSO_4$ formation.
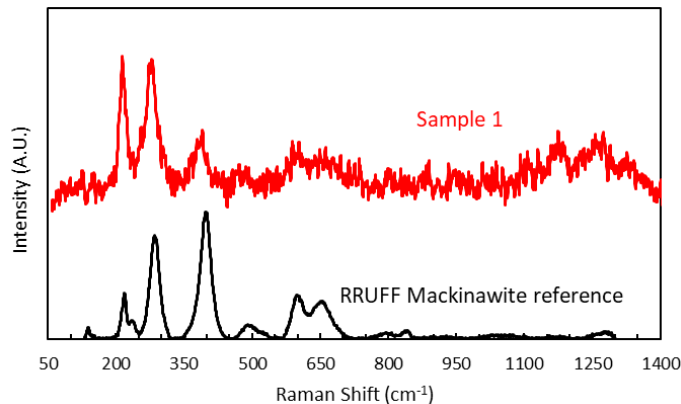
Figure 8: Raman spectroscopy of surface corrosion products after Test 4.

During all 4 experiments, the impurity concentrations of SO_2, NO_x, and H_2S were measured using gas detection tubes (error is +/-10%). The results are summarized in Figure 9. Tests 1, 2 and 3 had all impurities injected, but H_2S vanished almost immediately after reaching the test condition, and measured SO_2 is always higher than target value. Despite the possible SO_2 overdosing in the beginning of experiment, the trend generally agrees with reaction (4), where H_2S reacts with NO_2 and forms SO_2, NO, and H_2O. Eventually, after a series of reactions, H_2S would be consumed and support the formation of H_2SO_4. Therefore, the main corrosion product found was $FeSO_4$. During the experiment, H_2SO_4 could be dropped out following the series of reactions and the dropped out acid could accumulate on the horizontal surface and cause a more severe corrosion on the facing up side. In Test 4, reaction (1) could happen, and H_2SO_4 could form, but H_2S was always present in the system. Therefore, FeS formed as the main corrosion product at least in the outer layer.
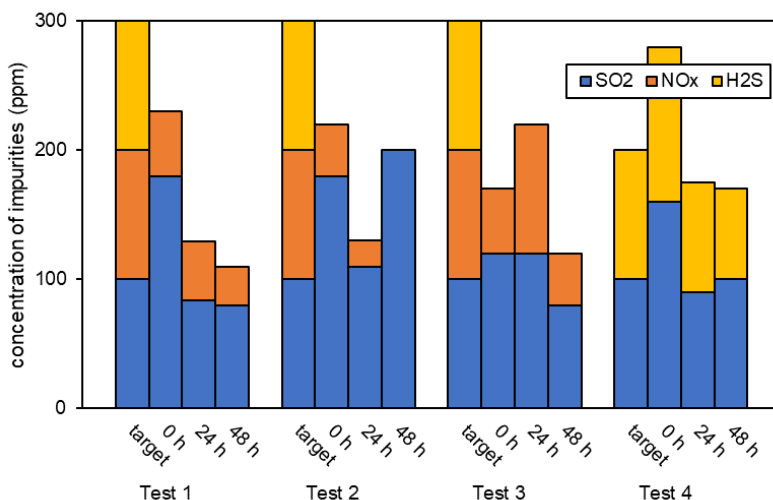
Figure 9: Impurity concentration changes during the experiment (measurement error +/-10%)

The corrosion rates of all samples in all 4 tests are plotted in Figure 10. Although the corrosion rates should not be compared among these tests since their conditions were all different and not comparable, the samples in each single test can be compared since these samples were all exposed to an identical environment. In the environment where H_2SO_4 was the most corrosive species, i.e. Tests 1, 2, and 3, the lower vertical samples experienced more corrosion, while the horizontal samples did not corrode differently from top to bottom. However, more corrosion products and more severe uniform corrosion were seen on the facing up sides of all samples in Test 3, which could be resulted from phased out H_2SO_4 during exposure that can remain on the horizontal surface and during depressurization. In Test 4,

samples placed horizontally experienced more corrosion at the bottom of the autoclave. However, in contrast to Test 3, both sides of the samples were corroded to the same extent in Test 4.
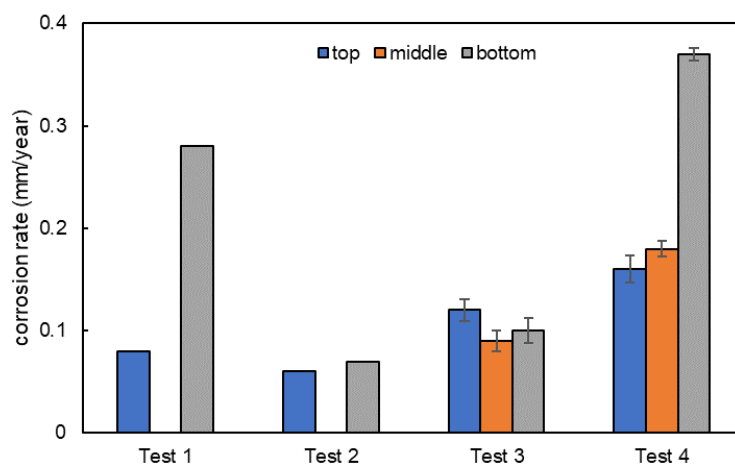
Figure 10: Corrosion rates of X65 exposed to supercritical CO_2 environment with impurities. Top and bottom samples in Test 1 and Test 2 refer to upper and lower samples, respectively. Error bars for Test 3 and Test 4 represent the max/min values of replicates.

SUMMARY

The corrosivity of dense phase CO_2 environment with impurities, including O_2, H_2S, SO_2, NO_2 (except Test 4), CH_4, H_2O, and N_2, were evaluated via four exposure experiments with X65 carbon steel specimens at 25 °C. The corrosion rate could be affected by sample position and orientation depending on the corrosive species. The bottom samples and facing up sides were more susceptible to corrosion. Main corrosion products found in the given environments were $FeSO_4$, FeS, and elemental sulfur. A recommendation based on this work to future CO_2 phase autoclave experiments is that sample locations should be considered whenever the autoclave allows multiple samples to be placed horizontally.

REFERENCES

1. B. H. Morland and A. Dugstad, "Corrosion of carbon steel in water equilibrated with liquid and supercritical CO2," CORROSION 2016, paper no. 7740 (Houston, TX: NACE, 2016).
2. A. Dugstad, M. Halseid, and B. Morland, "Experimental techniques used for corrosion testing in dense phase CO2 with flue gas impurities," CORROSION 2014, paper no. 4383 (Houston, TX: NACE, 2014).
3. B. H. Morland, T. Norby, M. Tjelta, and G. Svenningsen, "Effect of SO2, O2, NO2, and H2O concentrations on chemical reactions and corrosion of carbon steel in dense phase CO2," *Corrosion* 75, 11 (2019): p. 1327–1338.
4. B. H. Morland, A. Dugstad, M. Tjelta, and G. Svenningsen, "Formation of strong acids in dense phase CO2," CORROSION 2018, paper no. 11429 (Houston, TX: NACE, 2018).
5. Y. Xiang, M. Xu, and Y. S. Choi, "State-of-the-art overview of pipeline steel corrosion in impure dense CO2 for CCS transportation: mechanisms and models," *Corrosion Engineering, Science and Technology* 52, 7 (2017): p. 485–509.
6. B. H. Morland and G. Svenningsen, "Pitfalls and Artefacts in Corrosion Experiments with Dense Phase CO2," CORROSION 2021, paper no. C2021-16667 (Houston, TX: AMPP, 2021).
7. Y.S. Choi and S. Nesic, " Determining the corrosive potential of CO_2 transport pipeline in high pCO_2–water environments," *International Journal of Greenhouse Gas Control* 5, 4 (2011): p. 788–797.

8.   ASTM G1-03, "Standard Practice for Preparing, Cleaning, and Evaluating Corrosion Test Specimens" (West Conshohocken, PA: ASTM).

9.   B. Lafurente, R. Downs, H. Yang, and N. Stone, "The power of databases: the RRUFF project," in *Highlights in Mineralogical Crystallography*, T. Armbruster and R. Danisi, Eds. Berlin, Germany: De Gruyter, 2015, pp. 1–30.

10. B. H. Morland, A. Dugstad, and G. Svenningsen, "Experimental based CO2 transport specification ensuring material integrity," *International Journal of Greenhouse Gas Control* 119 (2022): p. 1–10.